Gaussian finite-element mixed-basis method for electronic structure calculations

Shunsuke Yamakawa* and Shi-aki Hyodo
Toyota Central R&D Labs., Inc., Nagakute, Aichi 480-1192, Japan
(Received 28 June 2004; revised manuscript received 8 October 2004; published 26 January 2005)

As a fully flexible basis function, the finite element (FE) function was introduced for the representation of the wave function in the molecular electronic state calculation within the density functional theory. The most serious disadvantage, which hindered the extensive application of the FE basis function, was the excessive computational cost for the representation of the core electron. In order to reduce this deficiency, the Gaussian-FE mixed basis method was proposed. The cooperation with Gaussian basis functions was utilized for representing the steeply varying part of the electronic wave function around the nuclei. Based on the results of the calculations for a set of small molecules, it was confirmed that the augmentation of the FE basis function using the Gaussian basis function allowed us to adopt a coarse uniform grid, and reduce the dependency on the relative configuration of FE nodal positions and atomic positions. These features were desirable to carry out the all-electron calculations of polyatomic molecules in the three-dimensional Cartesian coordinates while conserving the flexibility of the FE basis function.

DOI: 10.1103/PhysRevB.71.035113 PACS number(s): 31.15.Ew, 31.15.Ne, 02.70.Dh

I. INTRODUCTION

In the electronic state calculation, electronic wave functions are expanded in a set of one-electron functions. The atom-centered basis function is feasible for the expansion function because of the localized electron distributions of atoms or molecules. Gaussian basis sets[1] have been very successfully used in quantum-chemistry calculations. The improvement for the representation of molecular electronic wave functions is attained by the use of a large number of Gaussian basis sets consisting of the split-valence bases or functions of higher angular quantum numbers. However, in practical calculations, the basis is usually far from complete. Since the number of two-electron integrals rapidly grows as N^4, where N is the number of basis functions, excessive computational cost is required to obtain the basis-set limit for a given level of theory. This basic deficiency may be remarkably improved by using more flexible basis functions.

As an alternative approach for the molecular electronic state, the real-space grid method[2–12] has recently attracted increasing attention. The real-space grid method does not suffer from the same inefficiency problem concerning the number of two-electron integrals as the global basis sets because this method uses a strictly localized representation in the discrete element smaller than the entire simulation region for the electronic wave function. The finite-element method[2] (FEM) has been regarded as one of the possible real-space grid techniques to calculate electronic structures. In the FEM, the calculated region is represented as an assemblage of discrete elements interconnected at nodal points. The basis functions are strictly localized within each element. The main advantage of the FEM is its flexibility. The FEM can systematically improve the accuracy to the individual real space region by increasing the order of the basis function or using many elements for any electronic state under an inhomogeneous external field or under a complex boundary condition.

The finite difference method (FDM) is a means of numerically solving partial differential equations by using a finite value at the nodal points. The FDM for the electronic state calculations[11,12] has similar features to the FEM. Unlike FDM, however, an eigenstate in the FEM is calculated according to the variation principle. In the earliest examination, the FEM was applied to one- or two-dimensional calculations for an atom or a diatomic molecule, in which the symmetry could be used to reduce the dimensionality.[7–10] As a result, the FEM was proven to be suitable for highly accurate molecular orbital (MO) calculations. However, for three-dimensional cases, the system size will be obviously limited in this highly accurate MO calculation, since the number of nodal points must be extremely large. The very sharp variation in the wave function near the nucleus forces this problem to be more serious. Therefore, the availability of the FEM to practical electronic structure calculations essentially depends on the expressibility of the wave function near the nucleus.

Several efforts within the pure-FEM have been done to reduce the earlier-mentioned difficulty. The adaptive coordinate transformation,[5] in which the appropriate local resolution was accomplished by varying the grid spacing, has been adopted. However, the use of the mesh refinement technique alone does not accurately express the core electron. The pseudopotential technique combined with the mesh refinement technique is usually used in order to reduce the computational cost by the reduction of the explicitly treated orbital and by the availability of the coarse grid spacing.

On the other hand, the cooperation between the FE and atomic orbital type basis functions easily improves the accuracy more than the pure-FE basis set, because of the spherical symmetry of the electron distribution in a core region. Düsterhöft *et al.*[10] combined a numerical atomic orbital with a two-dimensional FEM and relativistically calculated the electronic structure of the C_2 molecule. This method showed better convergence for the ground state than the pure-FEM due to a better representation of the linear combinations of atomic orbital (LCAO) around the nuclei. It was an effective approach for representing the core region electrons. Unfortunately, full variational calculation in the combined basis

space was not carried out. Füsti-Molnar[13] divided the electronic wave function into the slowly and steeply varying parts in a three-dimensional space, and represented a respective region using the plane wave and the Gaussian basis function. The results of the calculations indicated that the electronic structure using the plane wave basis alone was sufficiently improved in the precision by combining the Gaussian basis function for the electronic structure calculations of molecules. The FEM is expected to show a similar behavior in combination with the Gaussian basis function. The coarse and fine grid spacings are analogous to adopting the low and high frequency terms of the plane wave, respectively. If the Gaussian basis function correctly represents the steeply varying part, the arrangement of the FEM can be set regardless of the atomic positions. Such a construction of the basis functions without a large number of grid points is expected to provide a simple procedure.

In order to make the FEM suitable for all-electron calculations of general molecules in three-dimensional Cartesian coordinates, the Gaussian-FE mixed basis method[14] was proposed. This mixed basis is composed of the linear combination of Gaussian basis functions and three-dimensional polynomials. This mixed method can be considered as the extension of the pure-FEM calculation for the quantum-chemistry calculations. The FE basis functions with a three-dimensional uniform coarse grid system are combined with the set of Gaussian basis functions, which are the components with a larger exponent of usual contracted Gaussian basis sets to correctly express wave functions near nuclei. The present construction of the basis functions is expedient in order to avoid considerable overlap between two different types of basis functions. In the FEM, the contribution from each element is assembled to construct the Fock matrix. The exchange potential based on the density functional theory (DFT) can be evaluated within each element. Therefore, the sparsity of the Fock matrix is ensured. In contrast, the exact Hartree-Fock exchange potential leads to the fully dense matrix, for which much more computational resources are required. In order to avoid the excessive calculation costs, all-electron calculations in the present investigation were carried out within the DFT. The variational problem was solved in this mixed-basis-function space.

In our previous work,[14] the Gaussian FE mixed-basis function method has examined as an electronic-state calculation technique for H_2, AlH, Al_2, and the Al_4H cluster. As a result of these calculations, the FE basis functions were found to automatically compensate for the part of the MO which cannot be represented by the Gaussian basis functions alone. Unfortunately, the effective construction of these functions with quite different natures has not yet been clarified. The objective of this work is to obtain the conditions under which the Gaussian basis function efficiently compensates the FE basis function without adversely affecting the accuracy of the wave functions.

The outline of this paper is as follows. In Sec. II the main characteristics of this mixed basis method are described. In Sec. III A we obtain the conditions that the slowly varying parts of the contracted Gaussian basis sets are successfully replaced by the FE basis functions through the electronic state calculations for H_2 and CO. In Sec. III B the total electron energies and dipole moments are calculated for a set of small test molecules using the derived condition. The accuracy and stability of this method are discussed in comparison with the results of the generally used Gaussian basis sets. The conclusions are given in Sec. IV, followed by the Appendix.

II. FORMULATION

The wave function was expanded as the linear combination of the Gaussian basis functions $\psi_G=(\varphi_{G1},\ldots,\varphi_{Gl})$ and the FE basis functions $\psi_F=(\varphi_{F1},\ldots,\varphi_{Fm})$:

$$\psi(\mathbf{r}) = \mathbf{C}\cdot\boldsymbol{\varphi}(\mathbf{r}), \tag{1}$$

where

$$\mathbf{C} = (C_{G1},\ldots,C_{Gl},C_{F1},\ldots,C_{Fm}), \tag{2}$$

$$\boldsymbol{\varphi} = (\psi_G,\psi_F) = (\varphi_{G1},\ldots,\varphi_{Gl},\varphi_{F1},\ldots,\varphi_{Fm}), \tag{3}$$

and $\mathbf{C}$ is the expansion coefficient vector. The piecewise polynomials of Lagrange type are defined as FE basis functions. Here, the one-dimensional case is considered for simplicity. The FE basis functions in nth element are expressed as

$$\psi_F^{(n)}(x) = \sum_{\alpha=1}^{k} C_\alpha^{(n)} S_\alpha^{(n)}(x), \tag{4}$$

where

$$S_\alpha^{(n)}(x) = \prod_{\substack{\beta=1\\(\beta\neq\alpha)}}^{k} \frac{(x-x_\beta^{(n)})}{(x_\alpha^{(n)}-x_\beta^{(n)})}, \tag{5}$$

and $S_\alpha^{(n)}$ is the αth local basis function defined in the nth element and $x_\alpha^{(n)}$ is the position of the nodal point with local number α. The global basis function φ_F is generated by assembling the local basis function S according to the nodal connectivity. As a result, φ_{Fi} is defined for the element involving the nodal point with global number i. The FE basis functions are adopted to represent the slowly varying part of the wave function. Within this condition, high-order FE basis functions are not necessarily required. The first- and second-order interpolation polynomials, which corresponded to $k=2$ and $k=3$ in Eq. (5), respectively, were evaluated as the FE basis functions. These functions are denoted by FE_{L1} and FE_{L2} hereafter. Higher dimensional FE basis functions are made by the product of the one-dimensional FE basis functions. Figure 1 shows the configurations of the nodal points in one element for each interpolation. The 20-nodal-point element, generally called the "serendipity" element,[15] was used for the second-order interpolation. The number of vertices of elements per dimension was 23. The grid spacings were set to 0.7 bohr except for the outer two grid spacings, which were set to 3.0 bohr. This calculating region was cubic with the size of 24.6 $bohr^3$. The Gaussian basis functions used here were defined as several parts of the usual 6-311G split valence type contracted Gaussian basis sets.[16,17]

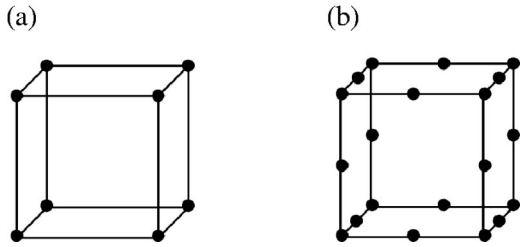

FIG. 1. Configuration of nodal points denoted by black dots in one cubic element for (a) the first order and (b) the second order interpolation polynomials.

The coefficient **C** was determined by consistently solving the following eigenvalue equation:

$$\mathbf{F}_{total} \cdot \mathbf{C} = \varepsilon \mathbf{U} \cdot \mathbf{C}, \tag{6}$$

where

$$\mathbf{F}_{total} = \mathbf{F}_{kin} + \mathbf{F}_{nucl} + \mathbf{F}_{el} + \mathbf{F}_{xc}, \tag{7}$$

$$\mathbf{F}_{kin} = \langle \psi_G | - \nabla^2 | \psi_{G'} \rangle + \langle \psi_G | - \nabla^2 | \psi_{F'} \rangle + \langle \psi_F | - \nabla^2 | \psi_{F'} \rangle, \tag{8}$$

$$\mathbf{F}_{nucl} = \langle \psi_G | V_{nucl} | \psi_{G'} \rangle + \langle \psi_G | V_{nucl} | \psi_{F'} \rangle + \langle \psi_F | V_{nucl} | \psi_{F'} \rangle, \tag{9}$$

$$\mathbf{F}_{el} = \langle \psi_G | V_{el} | \psi_{G'} \rangle + \langle \psi_G | V_{el} | \psi_{F'} \rangle + \langle \psi_F | V_{el} | \psi_{F'} \rangle, \tag{10}$$

$$\mathbf{F}_{xc} = \langle \psi_G | V_{xc} | \psi_{G'} \rangle + \langle \psi_G | V_{xc} | \psi_{F'} \rangle + \langle \psi_F | V_{xc} | \psi_{F'} \rangle, \tag{11}$$

$$\mathbf{U} = \langle \psi_G | \psi_{G'} \rangle + \langle \psi_G | \psi_{F'} \rangle + \langle \psi_F | \psi_{F'} \rangle, \tag{12}$$

and ε is the Lagrange multiplier. The integrations of each potential term including the FE basis functions were evaluated for every element. The contributions from all elements were assembled to construct the Hamiltonian matrix $\mathbf{F}_{total}$ and the overlap matrix **U**. The kinetic energy $\mathbf{F}_{kin}$ between Gaussian basis functions, which is the first term on the right-hand side of Eq. (8), was analytically calculated using the procedure of O-ohata *et al.*[18] The second and third terms were also analytically evaluated, since the three-dimensional (3D) integration for the FE basis functions reduced to the combination of one-dimensional (1D) integrations. The Coulomb potentials of the electron and core charge were separately calculated. The Coulomb potential $\mathbf{F}_{nucl}$ originating from the core charge was evaluated by using different procedures for each term on the right-hand side of Eq. (9). The first term is similarly evaluated for the kinetic energy term between Gaussian basis functions. In order to evaluate the second and third terms of Eq. (9), the potential within an element was separated into two parts. If there was no atomic center within an element, the Gauss-Legendre numerical integration gave a good result. The following relation[3] was used when a nucleus was located in the focused element:

$$\langle \varphi_F | V_{nucl} | \varphi_{F'} \rangle = \int \varphi_F(\mathbf{r}) \frac{Z_n}{|\mathbf{r} - \mathbf{R}_n|} \varphi_{F'}(\mathbf{r}) d\mathbf{r} = \frac{2Z_n}{\sqrt{\pi}} \int \frac{1}{w^2} [x_{FF'}] \times [y_{FF'}] \times [z_{FF'}] dw, \tag{13}$$

where

$$[x_{FF'}] = \int \varphi_{F_x}(x) \varphi_{F'_x}(x) \exp(-(x - X_n)^2 / w^2) dx, \tag{14}$$

and Z_n is the atomic number of the atom and $\mathbf{R}_n$ is the position of the nucleus. The integrals in the square brackets can be analytically evaluated. The integral with respect to w must be numerically done.

In order to evaluate the Coulomb potential $\mathbf{F}_{el}$ originating from the electron density, the Coulomb potential $V_{el}(\mathbf{r})$ of Eq. (10) is required. The $V_{el}(\mathbf{r})$ was evaluated by solving a Poisson's equation

$$\nabla^2 V_{el}(\mathbf{r}) = -4\pi\rho(\mathbf{r}), \tag{15}$$

where $\rho(\mathbf{r})$ is an electron density. Here, $V_{el}(\mathbf{r})$ was represented by the Gaussian FE mixed basis functions in the following form:

$$V_{el}(\mathbf{r}) = \sum_{i=1}^{l'+m} D_i \varphi'_i(\mathbf{r}), \tag{16}$$

where, D_i is the ith expansion coefficient, and φ'_i is the basis function for expressing $V_{el}(\mathbf{r})$. The same second-order FE basis functions as used for the electronic wave function, and Gaussian basis functions with squared exponents were used. In order to calculate Eq. (15), it is necessary to specify boundary conditions for the FE region. This was accomplished with a multipole expansion of $\rho(\mathbf{r})$ up to the quadrapole moments. Once $V_{el}(\mathbf{r})$ is obtained, $\mathbf{F}_{el}$ is analytically evaluated as triplet overlap integrals. All calculations described in this paper were performed using the DFT functional. The exchange functional proposed by Becke[19] and the correlation functional proposed by Lee, Yang, and Parr[20] were adopted here. The exchange correlation potential $\mathbf{F}_{xc}$ was evaluated by Gauss-Legendre numerical integration in each element. The generalized eigenvalue problem of Eq. (6) was solved by the conjugate-gradient (CG) method.[21]

III. RESULTS AND DISCUSSION

A. Electronic state of H_2 and CO

The accuracy and stability of the Gaussian FE mixed basis method were investigated for the electronic states of the H_2 and CO molecules. The configurations of the grid systems adopted for the calculations of H_2 are shown in Fig. 2. The numerical error originating from the adopted grid condition was evaluated for two different arrangements of grid points and atomic positions. The parameters of the Gaussian basis functions used here are listed in Table IV in the Appendix. In the mixed basis method, the FE basis functions show explicit contributions to part of a wave function, which is expressed by Gaussian components with a small exponent in a pure-Gaussian calculation. If the FE basis functions can replace a

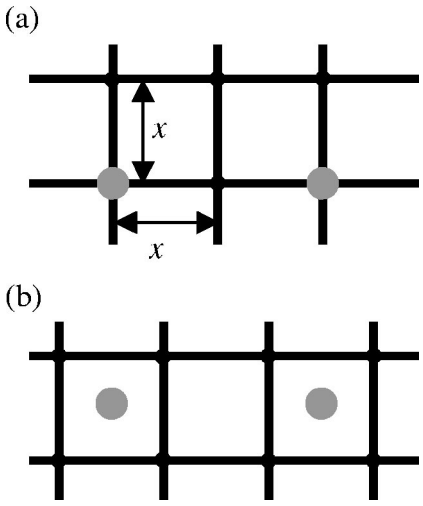

FIG. 2. Relative configuration of grid lines and hydrogen atoms denoted by gray circles. The atoms are located (a) on grid points or (b) at the centers of elements. The grid spacing x was set to 0.7 bohr.

part of the Gaussian basis set in the resultant electronic wave functions, the condition can be accepted as one equivalently accurate to the result from the pure-Gaussian procedure. The expressibility of the FE basis function to a part of Gaussian basis set was investigated by varying the value of the exponent of the Gaussian basis function. Such an investigation focused on an element involving a nucleus on a grid point. The criterion was evaluated through the estimation of deviations, which arose from the approximation for the *s*- and *p*-type Gaussian functions with exponent α, $f_G^\alpha(\mathbf{r})$, by the FE function $f_{FE}(\mathbf{r})$. The deviations were defined by

$$s(\alpha) = \sqrt{\frac{\int (f_G^\alpha(\mathbf{r}) - f_{FE}(\mathbf{r}))^2 d\mathbf{r}}{\int f_G^\alpha(\mathbf{r})^2 d\mathbf{r}}}. \qquad (17)$$

Figure 3 shows the deviation s as a function of the exponent of the Gaussian function α. The dependence of s on the order of the FE basis functions is also shown in Fig. 3. When a cubic element with the width of 0.7 bohr is used, the approximation by the FE_{L2} produces a smaller deviation than that by the FE_{L1}. The deviations in the FE_{L1} and FE_{L2} clearly arise where α is larger than 0.5 and 1.0, respectively. Table I shows the total electron energies for H_2 using various combinations. The total electron energies using the Gaussian FE basis set were compared with those using the 311G, 311+G(*p*) and augmented correlation consistent polarized valence quadruple zeta (aug-cc-pVQZ). The aug-cc-pVQZ basis set has a sufficient quality to discuss the Gaussian basis set limit. All calculations with the aug-cc-pVQZ basis set were performed using the GAUSSIAN03 program.[22] The accuracy of the energy is lost as the number of combined Gaussian basis functions decreases. The increase in the deviation s in Fig. 3 obviously correlates with the loss of accuracy. The FE_{L2} significantly improved the accuracy more than FE_{L1}.

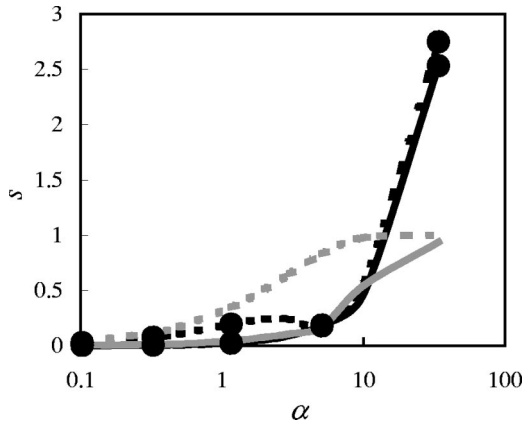

FIG. 3. Deviation $s(\alpha)$ caused by the approximation of FE function for the Gaussian function with various exponents α. Black and gray lines denote the deviation for the *s*- and *p*-type Gaussian functions, respectively. Dashed and solid lines are the values using first-order FE basis functions and using the second-order FE basis functions, respectively. The filled circles on each line of the *s*-type function denote the $s(\alpha)$'s at exponents of components of the 311G basis set for the hydrogen atom. The grid spacing was set to 0.7 bohr.

Figure 4 shows the relative contribution of each basis function to the electron density of H_2 for various combinations. The contributions of the FE basis functions decrease as those of the Gaussian basis functions increase. In the case of FE_{L1}, the contribution of ψ^2_{Gauss} should be more than 80% in order to reach a precision equivalent to the pure 311+G(*p*). In contrast, a Gaussian contribution of only 10% is required in the case of the FE_{L2}. As shown in Fig. 5, the contribution of the FE basis functions in 311G-FE_{L2} still remains in the middle of the H−H bond where the pure 311G cannot represent accurately. As a result, the 311G-FE_{L2} combination

TABLE I. The total electron energies for H_2 located on the grid point using various Gaussian FE basis sets and the conventional Gaussian basis sets. The values for H_2 located at the center of the element are given in parentheses.

	E[a]/Hartree	
N_G[b]	Gaussian FE_{L1}	Gaussian FE_{L2}
0	−1.8192 (−1.7599)	−1.8699 (−1.8613)
1	−1.8196 (−1.7806)	−1.8718 (−1.8745)
2	−1.8339 (−1.8388)	−1.8830 (−1.8824)
3	−1.8758 (−1.8758)	−1.8841 (−1.8840)
4	−1.8832 (−1.8833)	−1.8842 (−1.8842)
5	−1.8835 (−1.8834)	−1.8842 (−1.8842)
311G	−1.8809	
311+G(p)	−1.8834	
aug-cc-pVQZ	−1.8844	

[a]The geometry parameter was r(H−H)=1.4 bohr.
[b]Number of Gaussian basis functions combined with FE basis functions, as shown in the Appendix.

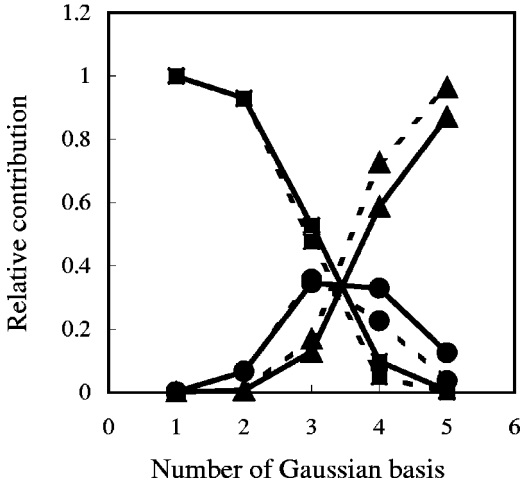

FIG. 4. Relative contributions of Gaussian and FE basis part for various combinations: Dashed lines denote the results using first-order FE basis functions, and solid lines denote those using second-order FE basis functions. The symbols ■, ●, and ▲ correspond to the contributions of ψ_{FE}^2, $\psi_{FE}\psi_G$, and ψ_G^2, respectively.

can reach a precision equivalent to the aug-cc-pVQZ. In order to investigate the dependence of the stability of the calculation on the arrangements of grid points and atomic positions, hydrogen atoms were located at the center of the element as shown in Fig. 2. As shown in Table I, the accuracy does not depend on the position of the nucleus, if the FE basis functions can replace a part of the Gaussian basis in a condition with a small deviation. In contrast, the accuracy fluctuated for the inadequate combinations.

The augmentation of FE basis functions using Gaussian basis functions, which can secure an equivalent precision to the pure-Gaussian basis set, was examined. For this purpose, it is important that the FE basis can fully replace a part of the Gaussian basis set in the electronic wave functions. The FE_{L2} can carry a much higher percentage of the contribution to the molecular orbital than the FE_{L1}.

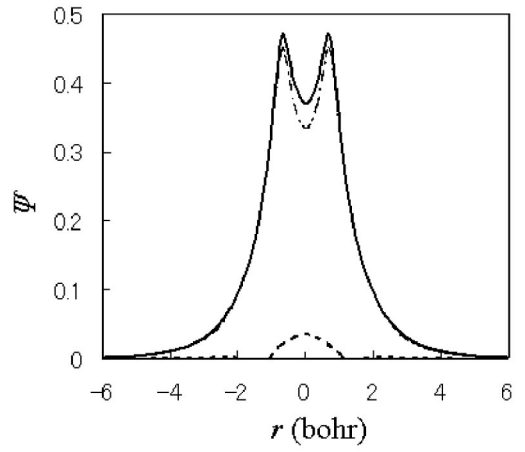

FIG. 5. Molecular orbital $\psi(\mathbf{r})$ on a molecular axis of H_2 using full 311G-FE_{L2}. The solid, dash-dot, and dashed line denote the molecular orbital, the contribution of the Gaussian basis functions, and the contribution of FE basis functions, respectively.

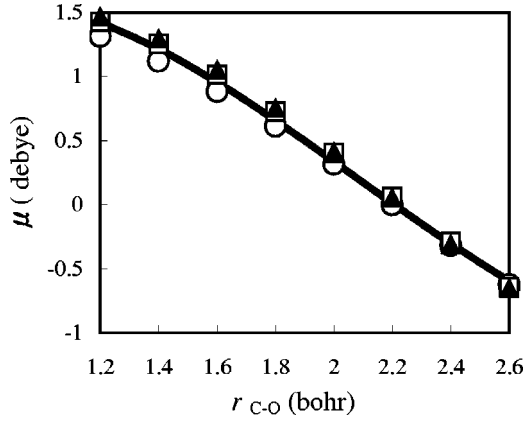

FIG. 6. Dipole moments for CO calculated with ○, 6-311G; ▲, 6-311+G(2*d*); and □, 6-3G-FE_{L2}. The solid line denotes the experimental dipole moment function (see Ref. 23). The 6-3G extracted from the 6-311G basis set for C and O was combined with the second-order FE basis functions.

The Gaussian FE mixed basis method was next applied to the calculation of the dipole moment of the CO molecule in order to investigate the expressibility of the FE basis function to Gaussian basis sets containing various components besides the *s*-type function. The dipole moment was discussed as a function of the CO bond length. The FE_{L2} was combined with the 6-3G corresponding to a part of the 6-311G basis set. Under this condition, the largest exponent of the replaced component in the 6-311G is about 0.48. As for the FE_{L2} with the grid spacing of 0.7 bohr, the deviation for the *s*- or *p*-type Gaussian function with this exponent remains as the small value as shown in Fig. 3. Therefore, the FE_{L2} is expected to have enough performance to represent the replaced component in the 6-311G basis set. As shown in Fig. 6, the calculation of the 6-3G-FE_{L2} results in a dipole moment equivalent to that of the 6-311+G(2*d*) basis set although the grid spacing is uniformly set regardless of the atomic positions. Figure 7 shows the difference in the molecular orbital between the 6-311+G(2*d*) and the 6-3G-FE_{L2}, and that between the 6-311G and the 6-3G-FE_{L2}. Figures 7(a) and 7(b) show the contour maps for the difference: $\Delta\psi=\psi$(6-3G-FE_{L2})-ψ(6-311G) in the lowest-energy orbital and the highest occupied molecular orbital (HOMO), respectively, while Figs. 7(c) and 7(d) show those for the difference: $\Delta\psi=\psi$(6-3G-FE_{L2})-ψ(6-311+G(2*d*)). The differences in the lowest-energy orbital [in Figs. 7(a) and 7(c)] are smaller than those in the HOMO [in Figs. 7(b) and 7(d)]. In particular, the differences in the HOMO show a positive value in the interatomic region, as shown in Figs. 7(b) and 7(d). This is mainly because the FE basis functions improve the expression of the wave function in the interatomic region due to the flexibility of the function.

As for the region apart from the core, the difference in Fig. 7(d) is smaller than that in Fig. 7(b). In the calculation with the 6-3G-FE_{L2}, the contributions of $\psi_{6\text{-}3G}^2$, ψ_{FE}^2, and $\psi_{6\text{-}3G}\psi_{FE}$ were 35.37%, 60.68%, and 3.95%, respectively. Obviously, the FE_{L2} carried a much higher percentage of the contribution to the molecular orbital than the Gaussian basis functions, and the region except for the core region was al-

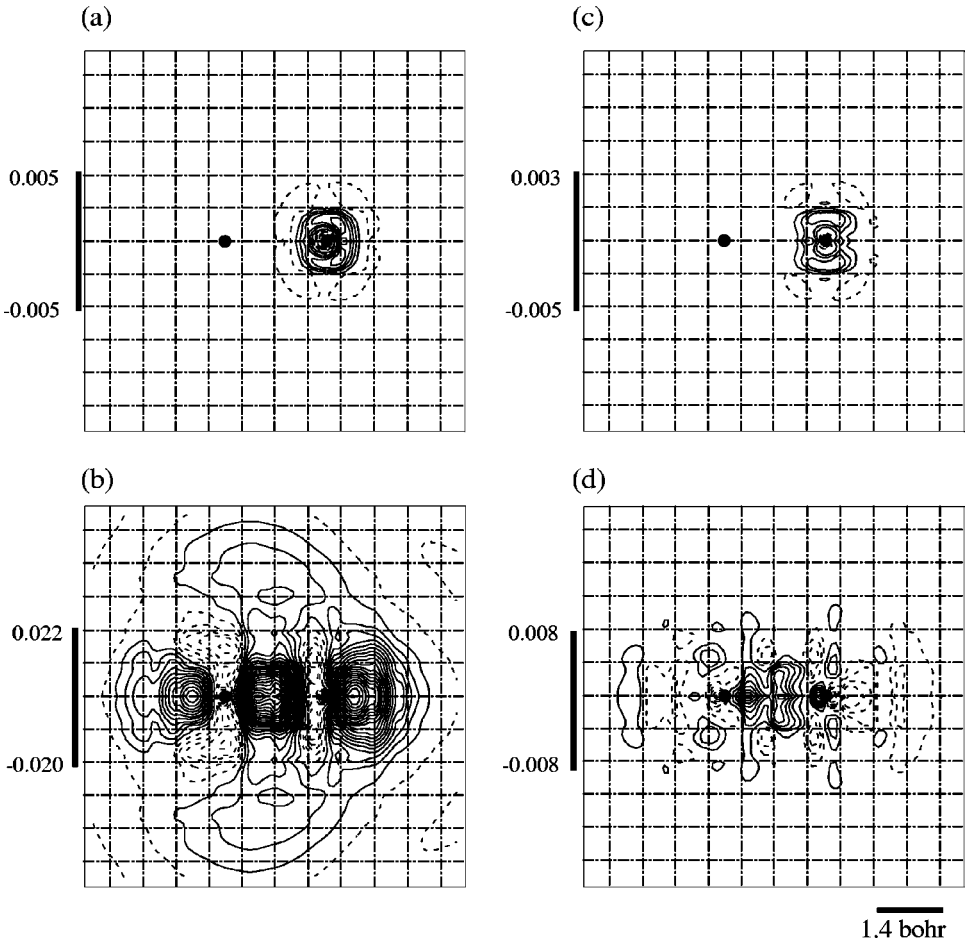

FIG. 7. Contour maps of the molecular orbital difference for CO [at r(C-O)=2.132 bohr]. In the four figures, (a) and (b) show the maps of the lowest orbital and the HOMO, respectively, for the difference [Ψ(6-3G-FE$_{L2}$)-Ψ(6-311G)], while (c) and (d) show those for the difference [Ψ(6-3G-FE$_{L2}$)-Ψ(6-311+G(2d))]. The values on the left hand side of each figure show the varying range of the difference. The solid and dashed lines indicate positive and negative values, respectively. The increment of each contour line is 0.001. The black dot on the right-hand side in each inset denotes the position of the oxygen atom, and that on the left-hand side denotes the position of the carbon atom. Grid lines denote the configuration of each element.

most expressed by the FE basis functions. Therefore, the decrease of the difference in this region as shown in Fig. 7(d) is because the FE$_{L2}$ basis functions successfully perform the role of the polarization and diffuse functions in the 6-311+G(2d) basis set.

The FE basis functions can replace the various kinds of Gaussian basis functions if the steeply varying part is correctly represented by the combined Gaussian basis functions. The wideness of the part represented by the Gaussian basis functions depends on the expressibility of the FE basis function determined by grid spacing and the order of the FE function. The number of nodal points per dimension between nuclei adopted here was at most three. In spite of such a coarse grid, the FE$_{L2}$ can carry a much higher percentage of the molecular orbital than the Gaussian basis functions. Accordingly, the cooperation with the Gaussian basis functions allows us to adopt a coarse uniform grid spacing.

B. Electronic state of H_2O, NH_3, and C_6H_6

The Gaussian-FE mixed basis method is applied to several polyatomic molecules based on the conditions investigated in the previous section. The 3G extracted from the 311G basis set used for H and the 6-3G extracted from the 6-311G basis set used for N or O were combined with the FE$_{L2}$. Table II shows the total electron energies and dipole moments in the 6-3G-FE$_{L2}$ for H_2O and NH_3. The accuracy of the 6-3G-FE$_{L2}$ is discussed in comparison with the results of the pure-Gaussian basis sets. As shown in Table II, the dipole moments of the lone pair molecules depend on the basis set as compared with the experimental value and the aug-cc-pVQZ results. The 6-311++G(d,p) basis set is inadequate to represent the dipole moments of both molecules. Although the 6-311++G(2d,2p) basis set shows better results, the value is still large. In contrast, the dipole moment of the 6-3G-FE$_{L2}$ is close to the aug-cc-pVQZ results. These tendencies are probably due to the molecular orbital representation in the region apart from nuclei. The flexibility of the FE basis functions is effective in improving the representation like the calculation for CO. Consequently, the 6-3G-FE$_{L2}$ lowered the total electron energy more than 6-311++G(2d,2p). The total electron energy of the 6-3G-FE$_{L2}$, however, does not reach the value of aug-cc-pVQZ, mainly because of the inadequacy of the 6-3G component representing the steeply varying part.

The calculation for C_6H_6 with the 5-2G-FE$_{L2}$ was carried out in the off-grid-point condition of atoms. If the grid-point condition applied here is insufficient for the accurate expression to the electronic state, the resulting wave functions must have been distorted from the ideal distribution. Thus, the numerical error in the calculated dipole moment is a good quantity to check it. Table III shows the results of the total electron energies and dipole moments for C_6H_6. The dipole moment of the 5-2G-FE$_{L2}$ shows that there is no significant distortion of the electron distribution in spite of the off-grid-

TABLE II. Total electron energies and dipole moments for H_2O and NH_3 using the Gaussian FE basis set and the conventional Gaussian basis sets. The 3G extracted from the 311G basis set for H, and the 6-3G extracted from the 6-311G basis set were used for N or O.

	H_2O[a]		NH_3[b]	
Basis set	E/Hartree	μ/Debye	E/Hartree	μ/Debye
6-3G-FE_{L2}	−85.6409	1.801	−68.5158	1.476
6-311++G(d,p)	−85.6374	2.123	−68.5103	1.721
6-311++G($2d,2p$)	−85.6408	1.924	−68.5140	1.563
aug-cc-pVQZ	−85.6504	1.789	−68.5204	1.476
Experiment	−85.5958[c]	1.855[d]	−68.4568[c]	1.472[e]

[a]The geometry parameters were r(O-H)=0.9572 Å and θ(HOH)=104.5 deg in Ref. 24.
[b]The geometry parameters were r(N-H)=1.0124 Å and θ(HNH)=106.7 deg in Ref. 25.
[c]These values are the sum of atomic energies in Ref. 26, nuclear repulsion energies for the experimental geometry (in Refs. 24 and 25), and experimental atomization energies in Ref. 27.
[d]Reference 28.
[e]Reference 29.

point condition of atoms. Figure 8 shows the contributions of ψ_G^2, ψ_{FE}^2, and $\psi_G\psi_{FE}$ to the electron density for C_6H_6. It is clear that the 5-2G-FE_{L2} can lower the total electron energy more than the 6-311++G even if the ψ_G^2 part has the remarkable contribution only around the nuclei. Subsequently, the overlap between the Gaussian basis functions belonging to different atoms is not necessarily required to achieve the calculation more accurate than the 6-311++G. In this condition, the largest exponent of the replaced component in the 6-311G is about 1.8. As shown in Fig. 3, this component cannot be completely represented by FE_{L2} with the grid spacing of 0.7 bohr. It is easily expected that further improvement of the accuracy can be obtained by adopting finer grid spacings.

This mixed basis method shows three advantages through the present examinations in contrast with the mesh refinement techniques within the pure FEM. First, the excessive degree of freedom of the FE basis functions for expressing the wave function near the nucleus can be avoided by the benefit of the Gaussian basis functions. Second, the increase in the number of atoms does not directly lead to the increase in the number of FE basis functions, since there is no necessity to connect the position of a nodal point and an atom. This is a desirable feature in order to apply this mixed basis method to the large-scale electronic structure problem. The last is the unneccessariness of the pseudopotential. The core electron is explicitly expressed in this method by the benefit of the combination of Gaussian basis functions. Unfortunately, the suitability to the parallel computing of this mixed basis method is lower than that of the pure FEM because of the nonlocality of the Gaussian basis functions. However, a serious deficiency can be avoided by not using the broadly spreading Gaussian basis functions. In this context, the number of integrations between the Gaussian basis functions in this method is proportional to the number of atoms, because of no significant overlap between the Gaussian basis functions belonging to different atoms. In the view of the present author, the present method is expected to reduce the basis set superposition error, which frequently appears in the calculation of a molecular interaction. The reason for this fortunate expectation originates from the fact that the superposition of the Gaussian basis functions of two different nuclei is extremely small under the present calculation conditions. As an additional application of this mixed basis method, the nuclear cusp is fairly expressible under the condition of which dense nodal points are arranged near the area around the nuclei. This fact can be naturally imagined through the construction of a wave function near the nuclei by dense FE basis functions.

TABLE III. Total electron energy and dipole moment for C_6H_6 [The geometry parameters were r(C-C)=2.619 bohr, and r(C-H)=2.033 bohr.] using the Gaussian FE basis set and the conventional Gaussian basis sets. The 2G extracted from the 311G basis set for H, and the 5-2G extracted from the 6-311G basis set for C were used.

Basis set	E/Hartree	μ/Debye
5-2G-FE_{L2}	−437.0038	0.000
6-311G	−436.9516	0.000
6-311++G	−436.9545	0.000
6-311++G(d,p)	−437.0095	0.000
6-311++G($2d,2p$)	−437.0188	0.000
aug-cc-pVQZ	−437.0512	0.000

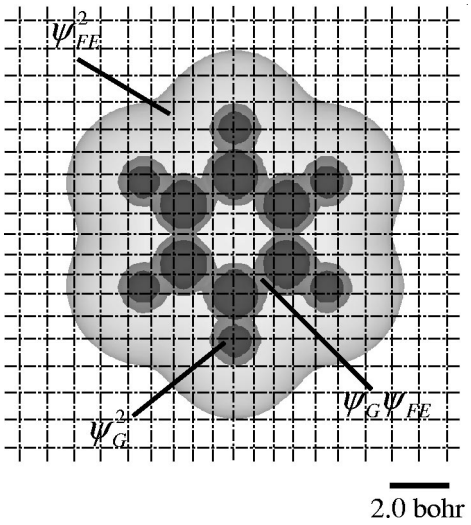

FIG. 8. Electron equidensity surface (at $\psi^2=1\times10^{-4}$) for C_6H_6.

IV. CONCLUSIONS

The flexibility of the FE basis functions is expected to be suitable for both highly accurate calculations and large systems. However, explicit applications have been less published because an excess degree of freedom is needed to

TABLE IV. Gaussian basis functions combined with FE basis functions.

Number of combining Gaussian basis functions	Exponents of combining Gaussian basis functions
0	
1	33.8650
2	5.09479, 33.8650
3	1.15879, 5.09479, 33.8650
4	0.325840, 1.15879, 5.09479, 33.8650
5	0.102741, 0.325840, 1.15879, 5.09479, 33.8650

represent the core electron. In order to propose an efficient solution of this problem, the Gaussian FE mixed basis method was proposed. The slowly varying part of the molecular orbital is represented by FE basis functions with a uniform coarse grid spacing, and the steeply varying part around a nucleus is represented by Gaussian basis functions, which have a contribution only around nuclei. The various conditions for combining the Gaussian basis functions with FE basis functions were examined in this work. The augmentation of the FE basis functions using Gaussian basis functions allows us to adopt a coarse uniform grid, and reduces the dependency of the FE nodal positions on atomic positions. The predominance over the pure FEM of this mixed basis method is that the augmentation can reduce the excess degree of freedom of the FE basis functions depending on the atomic position. Since the increase in the number of atoms does not directly lead to an increase in the number of the FE basis functions, this mixed basis method will provide a further extension of the FE basis method toward the all-electron calculation in a much larger system.

APPENDIX

As for the calculation of H_2, uncontracted Gaussian basis functions based on 311G were combined with FE basis functions. In order to certify the effectiveness of the contribution of the FE basis functions, Gaussian basis functions were uncontracted and the components with smaller exponents were excluded as shown in Table IV.

*Email address: e1044@mosk.tytlabs.co.jp

[1] A. Szabo and N. Ostlund, *Modern Quantum Chemistry* (Macmillan, New York, 1982).
[2] K.-J. Bathe and E. L. Wilson, *Numerical Methods in Finite Element Analysis* (Prentice-Hall, Englewood Cliffs, NJ, 1976).
[3] S. R. White, J. W. Wilkins, and M. P. Teter, Phys. Rev. B **39**, 5819 (1989).
[4] J. E. Pask, B. M. Klein, C. Y. Fong, and P. A. Sterne, Phys. Rev. B **59**, 12 352 (1999).
[5] E. Tsuchida and M. Tsukada, J. Phys. Soc. Jpn. **67**, 3844 (1998).
[6] T. L. Beck, Rev. Mod. Phys. **72**, 1041 (2000).
[7] F. S. Levin and J. Shertzer, Phys. Rev. A **32**, 3285 (1985).
[8] D. Sundholm and J. Olsen, Chem. Phys. Lett. **171**, 53 (1990).
[9] L. Yang, D. Heinemann, and D. Kolb, Phys. Rev. A **48**, 2700 (1993).
[10] C. Düsterhöft, D. Heinemann, and D. Kolb, Chem. Phys. Lett. **296**, 77 (1998).
[11] J. R. Chelikowsky, N. Troullier, and Y. Saad, Phys. Rev. Lett. **72**, 1240 (1994).
[12] H. Takahashi, T. Hori, H. Hashimoto, and T. Nitta, J. Comput. Chem. **22**, 1252 (2001).
[13] L. Füsti-Molnar and P. Pulay, J. Chem. Phys. **116**, 7795 (2002).
[14] S. Yamakawa and S. Hyodo, J. Alloys Compd. **356**, 231 (2003).
[15] See, e.g., Ref. 2, pp. 71–171.
[16] R. Krishnan, J. S. Binkley, R. Seeger, and J. A. Pople, J. Chem. Phys. **72**, 650 (1980).
[17] T. Clark, J. Chandrasekhar, G. W. Spitznagel, and P. von R. Schleyer, J. Comput. Chem. **4**, 294 (1983).
[18] K. O-ohata, H. Taketa, and S. Huzinaga, J. Phys. Soc. Jpn. **21**, 2306 (1966); **21**, 2313 (1966).
[19] A. D. Becke, Phys. Rev. A **38**, 3098 (1988).
[20] C. Lee, W. Yang, and R. G. Parr, Phys. Rev. B **37**, 785 (1988).
[21] C. K. Gan, P. D. Haynes, and M. C. Payne, Comput. Phys. Commun. **134**, 33 (2001).
[22] M. J. Frisch, G. W. Trucks, H. B. Schlegel, G. E. Scuseria, M. A. Robb, J. R. Cheeseman, J. A. Montgomery, Jr., T. Vreven, K. N. Kudin, J. C. Burant, J. M. Millam, S. S. Iyengar, J. Tomasi, V. Barone, B. Mennucci, M. Cossi, G. Scalmani, N. Rega, G. A. Petersson, H. Nakatsuji, M. Hada, M. Ehara, K. Toyota, R. Fukuda, J. Hasegawa, M. Ishida, T. Nakajima, Y. Honda, O. Kitao, H. Nakai, M. Klene, X. Li, J. E. Knox, H. P. Hratchian, J. B. Cross, C. Adamo, J. Jaramillo, R. Gomperts, R. E. Stratmann, O. Yazyev, A. J. Austin, R. Cammi, C. Pomelli, J. W. Ochterski, P. Y. Ayala, K. Morokuma, G. A. Voth, P. Salvador, J. J. Dannenberg, V. G. Zakrzewski, S. Dapprich, A. D. Daniels, M. C. Strain, O. Farkas, D. K. Malick, A. D. Rabuck, K. Raghavachari, J. B. Foresman, J. V. Ortiz, Q. Cui, A. G. Baboul, S. Clifford, J. Cioslowski, B. B. Stefanov, G. Liu, A. Liashenko, P. Piskorz, I. Komaromi, R. L. Martin, D. J. Fox, T. Keith, M. A. Al-Laham, C. Y. Peng, A. Nanayakkara, M. Challacombe, P. M. W. Gill, B. Johnson, W. Chen, M. W. Wong, C. Gonzalez, and J. A. Pople, GAUSSIAN 03, Revision B.02, Gaussian, Inc., Pittsburgh PA, 2003.

[23] I. Suzuki, Bull. Chem. Soc. Jpn. **45**, 2429 (1972).
[24] W. S. Benedict, N. Gailer, and E. K. Plyler, J. Chem. Phys. **24**, 1139 (1956).
[25] W. S. Benedict and E. K. Plyler, Can. J. Phys. **35**, 1235 (1957).
[26] E. R. Davidson, S. A. Hagstrom, S. J. Chakravorty, V. M. Umar, and C. F. Fischer, Phys. Rev. A **44**, 7071 (1991).
[27] M. W. Chase, Jr., *NIST-JANAF Thermochemical Tables*, 4th ed. (ACS, AIP, NIST, Washington, DC, 1998).
[28] S. A. Clough, Y. Beers, G. P. Klein, and L. S. Rothman, J. Chem. Phys. **59**, 2254 (1973).
[29] K. Tanaka, H. Ito, and T. Tanaka, J. Chem. Phys. **87**, 1557 (1987).